

Dislocations in metals and alloys with the hexagonal close-packed structure

H. Numakura and M. Koiwa

Department of Materials Science and Engineering, Kyoto University,
Sakyo-ku, Kyoto 606-8501, Japan

Abstract

Atomistic aspects of dislocations in hexagonal close-packed metals are reviewed. Computer simulation studies on the atomic structure of planar faults and dislocation cores have made essential contributions to understanding the wide variety of the plastic deformation behaviour of this class of materials. Stacking faults have been found to be the most important factor governing the core structure and the glide mechanism of dislocations; the preference for the glide plane, the magnitudes of flow stress and the deformation microstructure in various metals can be understood from the stability of the stacking faults in each material. A brief summary of the deformation behaviour of DO_{19} ordered alloys and intermetallic compounds is also given, focussing on Ti_3Al .

Riassunto

Vengono rivisti gli aspetti atomistici delle dislocazioni nei metalli esagonali compatti. Gli studi di simulazione al computer sulla struttura atomica dei difetti planari e dei nuclei di dislocazione hanno portato dei contributi essenziali alla conoscenza della grande variabilità del comportamento alla deformazione plastica di questa classe di materiali. Si è visto che i difetti di impilaggio costituiscono il fattore più importante nella determinazione della struttura del nucleo e del meccanismo di scorrimento delle dislocazioni: infatti dalla stabilità di detti difetti in ciascun materiale si può desumere nei vari metalli la preferenza per il piano di scorrimento, le grandezze della sollecitazione al flusso e la microstruttura di deformazione. Inoltre viene riassunto in breve il comportamento alla deformazione delle leghe ordinate DO_{19} e dei composti intermetallici, con particolare attenzione al Ti_3Al .

INTRODUCTION

Hexagonal close-packed (hcp) metals and alloys constitute an important class of engineering materials: titanium, with high specific strength and superior corrosion resistance, zirconium, with very low absorption of thermal neutrons, and the super-light-weight magnesium–lithium alloys. In recent years, Ti_3Al , an ordered compound of the hcp-based DO_{19} structure, has been attracting much attention in the research and development of high-temperature intermetallics.

Although single crystals of hcp metals deform extensively by slip deformation, polycrystals generally exhibit poor ductility. This problem is inherent to the crystal structure: the slip along the a axis direction, which is the primary deformation mode in all hcp metals, cannot give rise to strain along the c axis. The a slip is not the only mode of plastic deformation, however; a variety of deformation modes, i.e., secondary slip

modes and deformation twinning, are observed, the ease of such modes being different from one metal to another. Aiming to understand the broad spectrum of the plasticity, computer simulation studies of stacking faults and dislocation core structures have been carried out since the 1970s. In this article, we review the structures and glide mechanism at an atomistic level revealed by those investigations. Early simulation studies of dislocations were summarized by Minonishi [1] and by Vitek [2]. General reviews on the plasticity of hcp metals are found in the literature [3,4].

Deformation twinning is not discussed here, although it is another important mode of plastic deformation of hcp metals. Reviews on twinning in hcp metals are also available [5,6]. Recent progress in the research on this subject can be found in reference 7.

DEFORMATION MODES [3,4,8,9]

Figure 1 shows the slip systems observed for hcp metals. The slip in the $\langle \bar{1}\bar{1}20 \rangle$ direction (**a** slip) is the principal mode of deformation with the slip plane being the basal plane, (0002), in some metals and the prismatic plane, $\{ \bar{1}\bar{1}00 \}$, in others. The $\langle \bar{1}\bar{1}23 \rangle$ slip (**a+c** slip) occurs on the pyramidal planes, $\{ 10\bar{1}1 \}$ and $\{ 11\bar{2}2 \}$, and is observed in a number of hcp metals as a secondary slip mode contributing to the strain in the **c** axis direction.

The slip modes of common hcp metals are summarized in

Table 1. Metals such as beryllium, magnesium, zinc and cobalt deform primarily by the basal slip, while titanium, zirconium and some other transition metals deform primarily by the prismatic slip. The two groups of metals are referred to as basal-slip metals and prismatic-slip metals, respectively. The slip plane of **a+c** dislocations is $\{ 11\bar{2}2 \}$ for most of the basal-slip metals, while it is $\{ 10\bar{1}1 \}$ for titanium and zirconium. For titanium, slip on $\{ 11\bar{2}2 \}$ has also been reported [10,11].

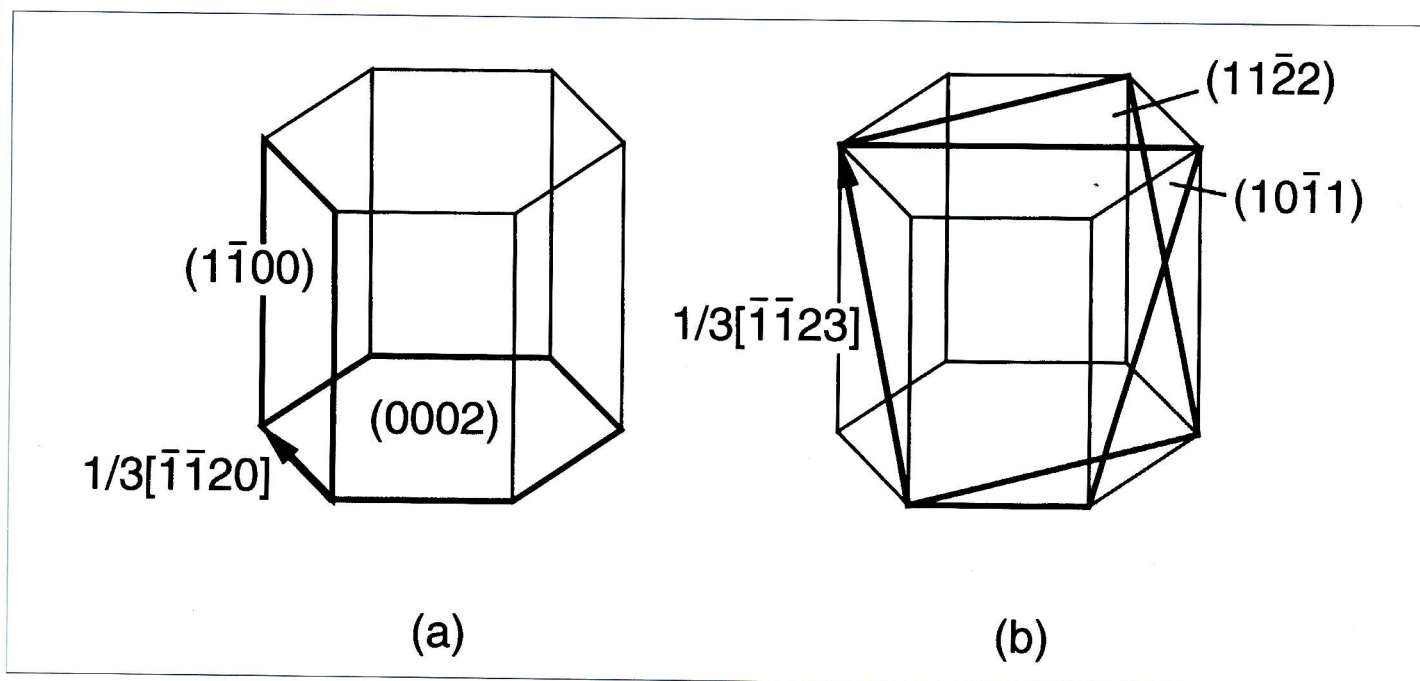


Figure 1: Slip systems in hcp metals. (a) **a** slip, (b) **a+c** slip

PROPERTIES OF **<A>** DISLOCATIONS

Experimental observations

The properties of **a** dislocations are outlined here by taking magnesium and titanium as representative materials of basal-slip metals and prismatic-slip metals, respectively; experiments on plastic deformation have been made most extensively for these two.

Figure 2 shows the critical resolved-shear-stress (CRSS) for the basal slip and prismatic slip in magnesium [12–14]. The CRSS for the basal slip is very low and is almost independent of temperature. The magnitude of the CRSS extrapolated to absolute zero temperature is about 1 MPa, which can be expressed as $5 \times 10^{-5} \mu$ in terms of the shear modulus of the material ($\mu \approx 19$ GPa). At low temperatures the CRSS for

the prismatic slip is two orders of magnitude higher than the CRSS for the basal slip.

Figure 3 shows the CRSS for the two slip systems in titanium [15–18]. In this material, the slip occurs more easily on the prismatic plane. The CRSS for the prismatic slip increases with decreasing temperature and reaches $1.4 \times 10^{-3} \mu$. That for the basal slip varies with temperature even more rapidly. It should be noted that commercially available titanium contains fairly large amounts of impurities. The contents of oxygen and iron, which are major impurity elements in titanium, in the materials used in the experiments compiled in Fig. 3 were 400 to 600 mol ppm and 30 to 50 of mol ppm, respectively. The CRSS for the prismatic slip in materials of lower oxygen concentrations has been found to be significantly lower [19].

In general, basal slip in magnesium, as well as in other basal-

slip metals, occurs without significant hardening, exhibiting sharp and regular slip lines, up to shear strains of 100 to 300%. Observations by electron microscopy have shown that the microstructure of magnesium deformed by basal slip involves dipoles of edge dislocations curved smoothly [20,21], similarly to the case of $1/2\langle 110 \rangle$ dislocations in face-centred cubic (fcc) metals. In titanium, prismatic slip exhibits fine and straight slip lines [17], while basal slip is associated with wavy surface-markings [18]. When titanium is deformed by prismatic slip, screw dislocations are predominant in the microstructure, particularly at low temperatures [22,23]. These features are similar to those associated with $1/2\langle 111 \rangle$ dislocations in body-centred cubic (bcc) metals.

The distinctive behaviour of the slip in the two groups of metals, i.e., the relative ease of the basal and prismatic slip systems, was discussed on the basis of the Peierls-Nabarro model of dislocations [24,25]. In terms of the Peierls stress, which is the intrinsic lattice friction force against the dislocation motion, a dislocations are expected to glide on the basal plane more easily than on the prismatic plane when the anisotropy in shear moduli, $A = C_{44}/C_{66}$, is less than unity and the axial ratio c/a is larger than the ideal value, 1.633. In Table 1, this prediction is found to agree with experiment only for zinc and cadmium. Quantitatively, theoretical esti-

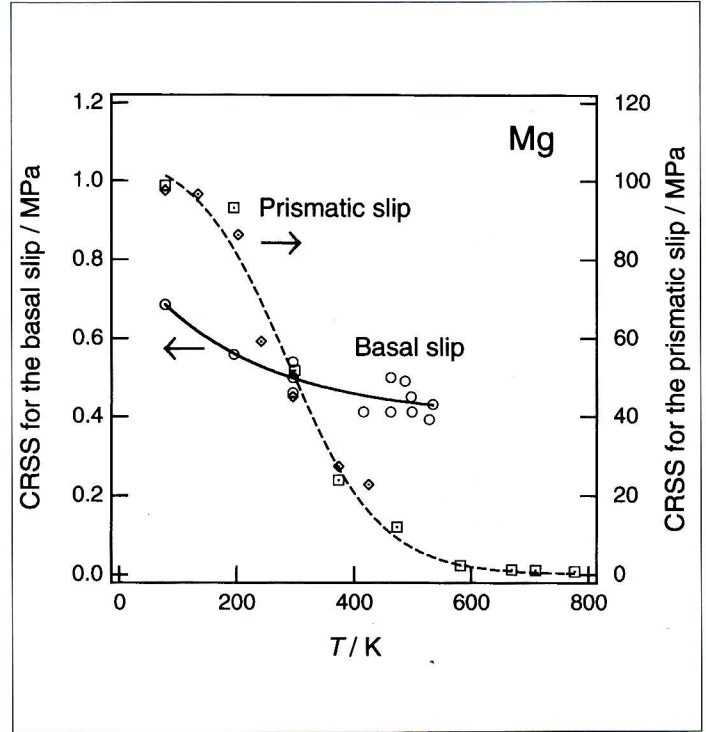


Figure 2: Critical resolved-shear-stress (CRSS) for the basal slip and the prismatic slip in magnesium [12-14]

TABLE 1 - Axial ratio c/a , shear anisotropy factor $A = 2C_{44}/(C_{11} - C_{12})$, and observed modes of slip deformation. Ln: lanthanoid

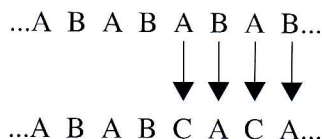
Group	Metal	c/a	A	a slip	$a+c$ slip
2	Be	1.568	1.22	$\{0002\}, \{10\bar{1}0\}$	$\{11\bar{2}2\}$
	Mg	1.624	0.97	$\{0002\}, \{10\bar{1}0\}, \{10\bar{1}1\}$	$\{11\bar{2}2\}$
3	Y	1.572	0.98	$\{10\bar{1}0\}, \{0002\}$	
4	Ti	1.587	1.33	$\{10\bar{1}0\}, \{0002\}, \{10\bar{1}1\}$	$\{10\bar{1}1\}, \{11\bar{2}2\}$
	Zr	1.593	0.91	$\{10\bar{1}0\}, \{0002\}$	$\{10\bar{1}1\}, \{11\bar{2}2\}^\dagger$
	Hf	1.581	1.07	$\{10\bar{1}0\}, \{0002\}$	
7	Re	1.615	0.94	$\{0002\}^*, \{10\bar{1}0\}^*, \{10\bar{1}1\}^\ddagger$	
8	Ru	1.582	0.96	$\{10\bar{1}0\}, \{0002\}$	
9	Co	1.623	1.07	$\{0002\}$	$\{11\bar{2}2\}^\ddagger, \{11\bar{2}1\}^\S$
12	Zn	1.856	0.61	$\{0002\}, \{10\bar{1}0\}$	$\{11\bar{2}2\}$
	Cd	1.886	0.54	$\{0002\}$	$\{11\bar{2}2\}$
Ln	Gd	1.591	0.99	$\{10\bar{1}0\}, \{0002\}$	
	Tb	1.583		$\{10\bar{1}0\}, \{0002\}$	
	Dy	1.574	1.00	$\{10\bar{1}0\}, \{0002\}$	$\{11\bar{2}2\}$
	Ho	1.571		$\{10\bar{1}0\}, \{0002\}$	
	Er	1.571	1.00	$\{10\bar{1}0\}, \{0002\}$	

* The ease of $\{0002\}$ slip and that of $\{10\bar{1}0\}$ slip are close to each other. ‡ The slip direction has not been identified. § $a+c$ dislocations generated ahead of the tip of a $\{111\}$ twin.

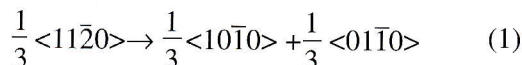
mate of the magnitude of the Peierls stress (for an edge dislocation) is $2 \times 10^{-3} \mu$ for the basal slip in magnesium and $1 \times 10^{-3} \mu$ for the prismatic slip in titanium. Although the latter agrees well with the experimental value, the former is about two orders of magnitude larger than that observed in experiment. It thus turns out difficult to explain the properties of **a** dislocations in various hcp metals by the Peierls-Nabarro model. In the 1970s, atomistic studies of dislocations led us to the recognition that dislocation core structures govern the plasticity of bcc metals [2]. It is likely that such core effects play an important role also in hcp metals. For example, the discrepancy between the calculated and experimental critical stress for the basal slip in magnesium strongly suggests that a dislocations do not exist in the form of a perfect dislocation.

Stacking faults and core structures of **a** dislocations on the basal plane

The intrinsic stacking fault I_2 on the basal plane is one of the planar faults directly relevant to **a** dislocations [26]. It corresponds to the change in the stacking sequence of the basal plane



This fault is predicted by the hard-sphere model and is always stable owing to the crystal symmetry. An **a** dislocation may therefore dissociate into two Shockley partial dislocations on the basal plane bounding a ribbon of the fault in between:



This dissociation has been verified for cobalt by electron microscopy [27]. In other basal-slip metals, **a** dislocations are also expected to be extended similarly on the basal plane, even though the separation between the partial dislocations, which depends upon the magnitude of the stacking fault energy, may not be appreciably large. One can thus naturally understand the similarities between the experimental observations for the basal-slip metals and those for fcc metals. The stacking fault energies of some selected hcp metals are listed in Table 2 [3,27,28]; they have been estimated from the dissociation width of **a** dislocations or from the flow stress in experiments of work-hardening. The energy of I_2 is of the order of 100 mJ/m² except for cobalt. Theoretical calculations tend to predict lower values than the experimental estimates; for example, a recent calculation based on the elec-

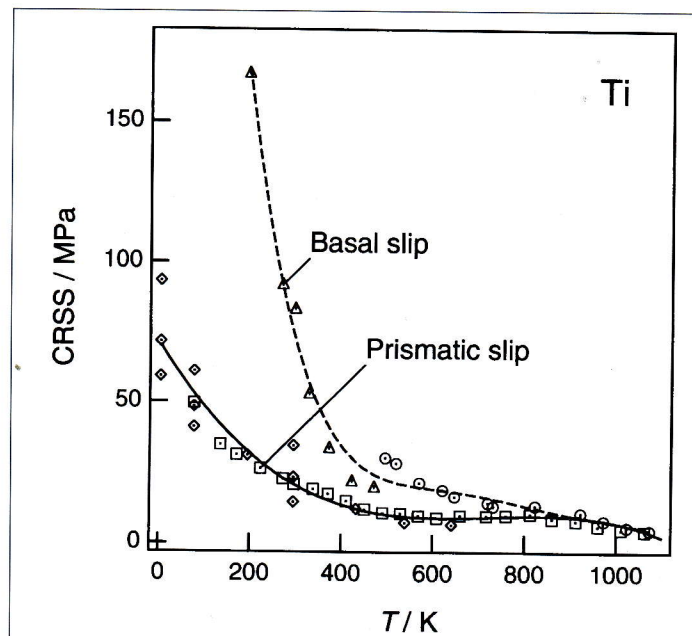


Figure 3: Critical resolved-shear-stress (CRSS) for the prismatic slip and the basal slip in titanium [15–18]

tron theory reports 54 mJ/m² for magnesium [29]. The first atomistic study of dislocations in hcp crystals was done by Basinski, Duesbery and Taylor in early 1970s [30,31]. They calculated the core structure of screw dislocations and the critical stress for glide motion in model crystals of hcp and bcc structures using a pseudopotential for sodium. In the hcp crystal, the **a** screw dislocation is extended on the basal plane according to reaction (1) and glides on the basal plane under an external shear stress of $5 \times 10^{-4} \mu$. On the other hand, the screw dislocation in the bcc crystal exhibits a displacement distribution of threefold symmetry, which is expected from the crystal structure. The critical stress for the glide motion was found to be as high as $10^{-2} \mu$. This comparative study contrasted the effect of crystal structure on the atomic structure and properties of dislocations. After this pioneering work, Bacon and coworkers performed detailed simulation studies of **a** dislocations in hcp crystals using various pairwise interatomic potentials [32–35]. The results obtained from different potentials are essentially similar to each other: **a** dislocations are always extended on the basal plane and glide most easily along the basal plane. This is a natural consequence of the fact that the basal stacking-fault energy is very low in the models based on pairwise potentials. As mentioned in the previous section, dipoles of basal edge dislocations are observed in magnesium deformed by basal slip. This arrangement is considered to result from annihila-

tion of screw segments of **a** dislocations by their cross-slip onto the prismatic plane. For a dislocation extended on the basal plane to cross-glide on the prismatic plane, the displacements spread over the basal plane need to constrict first. According to the simulation of the motion of **a** dislocations under external stresses by Bacon and Martin [33], when shear stress is applied on the prismatic plane, the two Shockley partial dislocations on the basal plane rejoin and then the dislocation begins to glide along the prismatic plane. The critical stress for the whole process is several times higher than that for the basal glide.

When constriction of an extended core occurs at a part of the dislocation line, a pair of kinks may be formed from there, out of the plane of the initial spreading. Then the segment can undergo cross-glide movement, as illustrated in Fig. 4 for the case of the cross-glide of an **a** screw dislocation from

the basal plane onto the prismatic plane [36]. Motion of a dislocation over long distances may occur by repetition of such a process, which involves the transformation of the core structure between extended (locked) and constricted (unlocked) configurations. This mechanism of the glide motion is referred to in the literature as the Friedel-Escaig mechanism or the pseudo-Peierls mechanism. Thermally-activated movements of **a** screw dislocations on non-basal planes, as well as those of screw dislocations in bcc metals, have often been discussed in terms of this mechanism [36,37]. Detailed in-situ electron microscopy studies on magnesium and beryllium have shown that the prismatic glide of **a** dislocations is actually controlled by the motion of screw segments; the observed features of the dislocation motion are in accordance with the picture of locking and unlocking [38].

TABLE 2 - Energies of the stacking faults on the basal plane (γ_B) and the prismatic plane (γ_P) estimated experimentally (Exp) [3,17,27,28,46,47] and those calculated theoretically (Calc) [50]. $R = (C_{66}/\gamma_P)/(C_{44}/\gamma_B)$ is the measure for the preference of the **a dislocation for prismatic slip to basal slip. B and P denote respectively the basal plane and prismatic plane**

Metal	γ_B (mJ/m ²)		γ_P (mJ/m ²)		R	Observed slip plane
	Exp	Calc	Exp	Calc		
Be	>230 ^a	390		620	0.5	B
Mg	78-280 ^a	30		125	0.25	B
Y		210		60	3.5	P
Ti	300 ^b	290	145 ^d - 150 ^e	110	2.5	P
Zr		340	56 ^f	150	2.3	P
Hf		390		185	2.1	P
Re		540		600	0.9	B, P
Ru		875		520	1.7	P
Co	27 ^c	45		230	0.2	B
Zn	74-300 ^a	35		210	0.25	B
Cd	105-205 ^a	15		150	0.2	B

References: a [28], b [3], c [27], d [17], e [46], f [47]

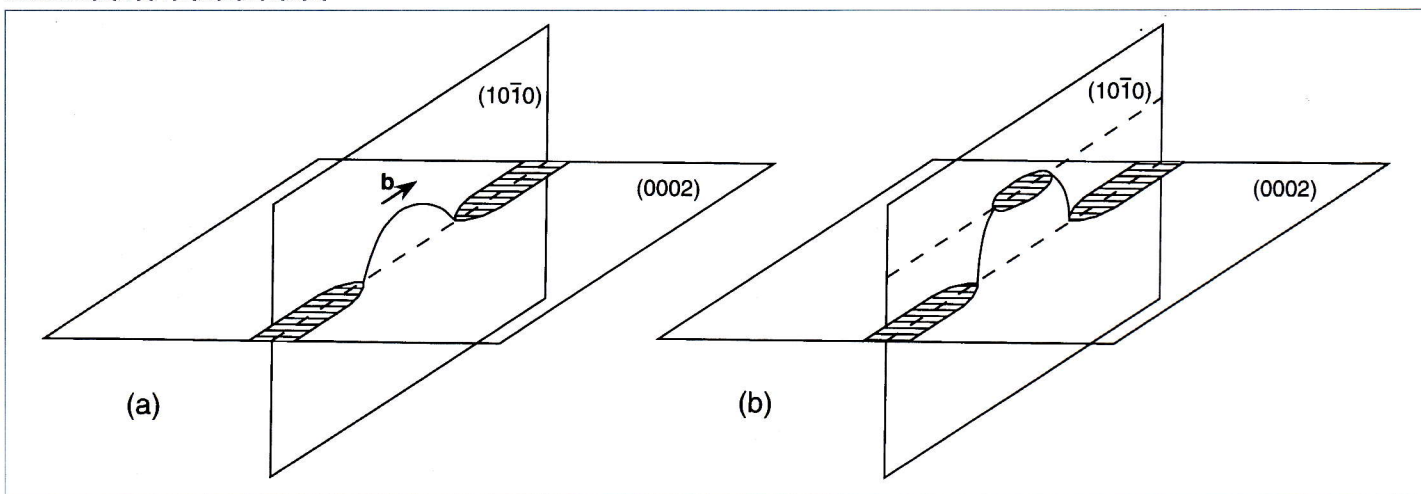


Figure 4: Glide motion along the prismatic plane of the **a** screw dislocation initially extended on the basal plane [36]. (a) A kink-pair bows out from a segment on which the basal extension is constricted. (b) The core is extended again on the basal plane after arriving at a stable position

Stacking faults and core structure of $\langle a \rangle$ dislocations on the prismatic plane

The fact that a dislocations glide more easily on the prismatic plane in some metals strongly suggests the presence of a low-energy stacking fault on the prismatic plane in such metals, through which the core can be extended over the prismatic plane. Possible stacking faults on the prismatic plane and dissociation of dislocations were studied on the basis of the hard-sphere model [24,39,40], where a stable fault with a translation vector $1/6\langle 11\bar{2}1 \rangle$ ($= a/2 + c/6$) was predicted. A possible scheme of the dissociation on the prismatic plane is thus

$$\frac{1}{3}\langle 11\bar{2}0 \rangle \rightarrow \frac{1}{6}\langle 11\bar{2}1 \rangle + \frac{1}{6}\langle 11\bar{2}\bar{1} \rangle, \quad (2)$$

which is illustrated in Fig. 5 in the form of a vector diagram. Regnier and Dupouy [41] proposed an alternative dissociation model into two collinear partial dislocations of unequal Burgers vectors:

$$\frac{1}{3}\langle 11\bar{2}0 \rangle \rightarrow \frac{1}{9}\langle 11\bar{2}0 \rangle + \frac{2}{9}\langle 11\bar{2}0 \rangle. \quad (3)$$

This model is based on the fact that most of the prismatic-slip metals take the bcc form at high temperatures; the atomic arrangement at the fault created by the dissociation is the same as that in the bcc structure.

Schwartzkopff [42] was the first to examine the stability of stacking faults in hcp crystals by atomistic simulation. He calculated the energies of translation faults on some low-index planes using a Morse potential to confirm the presence of the stacking faults predicted by the hard-sphere model and to discover some more. The translation vector $1/6\langle 11\bar{2}1 \rangle$ on the prismatic plane was found to correspond to an energy minimum, supporting reaction (2). Bacon and Liang [43] also calculated stacking fault energies using various pairwise potentials. Figure 6 shows a contour map of the energies of translation faults on the prismatic plane calculated using the Lennard-Jones potential truncated after 56 neighbour atoms [44], which is one of the four potentials employed by Bacon and Liang. An energy minimum is located at a position close to that predicted by the hard-sphere model, the energy being 13 times the energy of I_2 [45].

According to the simulation of dislocations using pairwise potentials by Liang and Bacon [34,35], an edge dislocation on the prismatic plane exhibits a core structure in which the distribution of displacements is confined at the centre, which is similar to that calculated by elasticity theory, when the displacement field for a perfect dislocation is given as the initial condition. When the calculation is started with the initial displacement distribution corresponding to an extended dislocation of the right hand side of reaction (2), on the other hand, the extended core with the stacking fault on the prismatic plane is retained. The spreading is, however, much

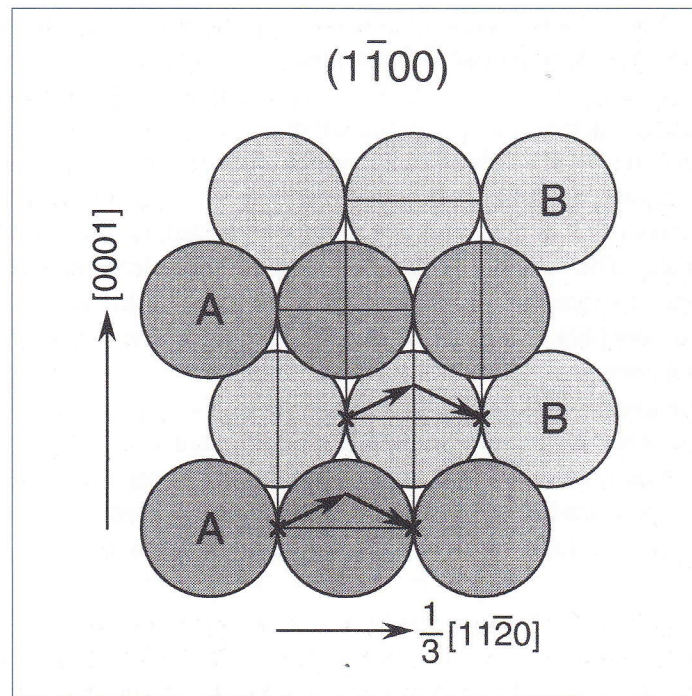


Figure 5: Atomic arrangement of the $(1\bar{1}00)$ prismatic plane. Atom rows B are located below rows A by $1/3$ times the interplanar spacing. Crosses indicate the positions of atoms in the next plane. Arrows represent the dissociation of the a dislocation on the prismatic plane predicted by the hard-sphere model

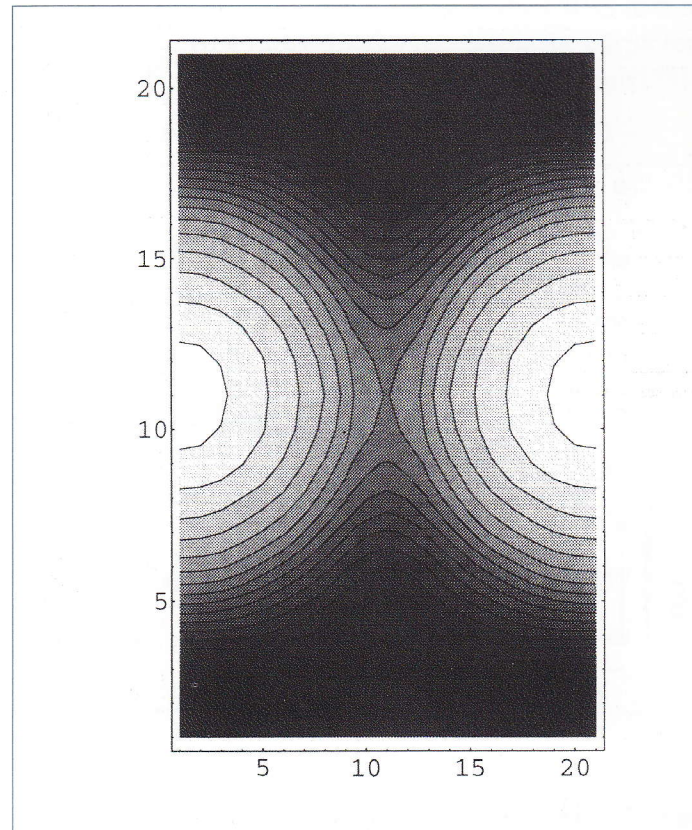


Figure 6: Energy contour map for a planar fault produced by a shear displacement on the prismatic plane calculated using the Lennard-Jones potential [44]. The area shown here corresponds to the rectangle in Fig. 5. Darker part is lower in energy

narrower than the case of the edge dislocation dissociated into Shockley partial dislocations on the basal plane [34], and the critical stress for the glide motion is about twice as high [35].

In real prismatic-slip metals such as titanium, the energy of the stacking fault on the prismatic plane is expected to be lower than, or at least close to, that of the fault on the basal plane. The stacking fault energy of the prismatic plane has been estimated from experiment for titanium [17,46] and zirconium [47], as shown in Table 2; in titanium it is about half the energy of I_2 . Since the energy of the basal fault is almost always the lowest with pairwise potentials, some other models of atomic interaction should be employed in order to simulate the prismatic-slip metals. Legrand [48] adopted a method of approach based on electron theory; he calculated the core structure of the **a** screw dislocation in titanium by the tight-binding approximation, by which localized anisotropic bonding associated with d-electrons can be taken into account. With this method, the energy of the stacking fault on the prismatic plane has been found to be lower than the energy of the basal fault I_2 . The calculated structure of the dislocation core is illustrated in Fig. 7, where the distribution of the displacements is schematically delineated. The dislocation is not dissociated into partial dislocations, and close inspection reveals that the screw displacements are spread primarily

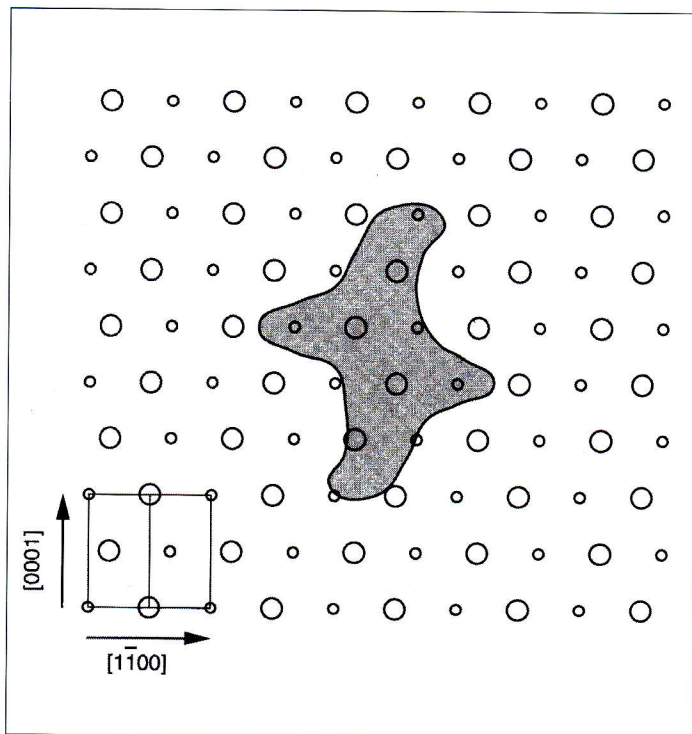


Figure 7: Schematic illustration of the distribution of the displacements in the calculated core structure of the **a** screw dislocation in titanium [48]

along the prismatic plane, reflecting the low energy of the prismatic stacking fault, and secondarily along the basal plane. For a dislocation with such a non-planar core structure to undergo glide motion, constriction of the displacements is necessary, whichever the glide plane is. Since the spreading is more extensive along the prismatic plane, the motion along the prismatic plane is expected to be easier. (However, simulation of glide motion has not been performed.) If dislocations in titanium exhibit such a core structure, the high CRSS and the strong dependence on temperature can be explained; the motion of the dislocations will be controlled by the pseudo-Peierls mechanism for both the glide on the prismatic plane and on the basal plane. In fact, the prismatic glide of **a** dislocations in titanium has been found to be controlled by the motion of screw segments, which travel by a repeated sequence of locking and unlocking [49].

Earlier than the study of the dislocation core structure, Legrand had calculated the stacking fault energies on the basal and prismatic planes in various hcp metals by adopting the pseudopotential method for divalent metals (beryllium, magnesium, zinc and cadmium) and the tight-binding method for others (transition metals) [50]. The results are summarized in Table 2: the stacking fault energy is lower for the basal plane in the divalent metals, whereas the relative magnitudes of the energies of the faults on the basal plane (γ_B) and on the prismatic plane (γ_P) vary with the number of d-electrons in the transition metals. The ratio of the shear modulus to the stacking fault energy, μ/γ , serves as a measure of the width of the splitting of a dislocation; the magnitudes of this quantity are compared for the prismatic plane and the basal plane. Since the motion of a dislocation extended more widely must be easier, prismatic glide will be favoured if the ratio, $R \equiv (C_{66}/\gamma_P)/(C_{44}/\gamma_B)$, is greater than unity, while basal glide will be favoured if opposite. The values of R for various metals are listed in the last column of Table 2. The predictions agree well with experiment; $R > 1$ for the prismatic-slip metals and $R < 1$ for the basal-slip metals.

More recently, the core structure of **a** dislocations has been studied using many-body potentials by Igarashi and coworkers. They developed Finnis-Sinclair type potentials for eight hcp metals (beryllium, magnesium, titanium, zirconium, hafnium, ruthenium, cobalt and zinc) that reproduce well the axial ratio and anisotropic elastic constants of each metal [51,52]. As it turned out, however, that the basal fault I_2 was the lowest in energy in all the eight models, none of them is a direct model of a prismatic-slip metal. Nevertheless, important insights on the nature of **a** dislocations have been gained from the simulation of core structures for the models of beryllium, magnesium and titanium [52,53], as summarized below.

In these models, two possible core configurations exist for the **a** screw dislocation, depending upon the initial condi-

tion; one is extended on the basal plane with the stacking fault I_2 and the other is extended on the prismatic plane. The latter can be written as

$$\frac{1}{3}\langle 11\bar{2}0 \rangle \rightarrow \frac{1}{6}\langle 11\bar{2}x \rangle + \frac{1}{6}\langle 11\bar{2}\bar{x} \rangle, \quad (4)$$

where $x \cong 0, 0.1$ and 0.15 for beryllium, magnesium and titanium, respectively. The structure extended on the prismatic plane is slightly more favourable in the models of beryllium and titanium, while that extended on the basal plane is far more favourable in the model of magnesium. The preference for the basal extension in the model of magnesium is natural because the energy of the stacking fault on the basal plane is much lower than that on the prismatic plane.

In the model of beryllium, the screw dislocation dissociates on the prismatic plane into two screw partial dislocations because the c component of the fault on the prismatic plane is virtually zero. With this configuration, it is easy for the

PROPERTIES OF $\langle A+C \rangle$ DISLOCATIONS

Experimental observations

Experimental studies of $a+c$ slip are usually conducted by preparing single-crystal specimens and subject them to loading along the c axis. However, it is not easy to investigate the properties of the dislocations in detail because twinning competes under uniaxial deformation in the c axis. Figure 8 shows some of the limited experimental results on the $a+c$ slip; the CRSS for the $\{11\bar{2}\}$ slip in magnesium [54,55] and that for the $\{10\bar{1}\}$ slip in a titanium–aluminium (7 mol % Al) solid solution alloy [56] are plotted against temperature. The CRSS is much higher than those for a slip (Figs 2 and 3), and they increase rapidly with decreasing temperature to reach the order of $10^{-2} \mu$ at low temperatures.

In the deformation microstructure of titanium [9,22], titanium–aluminium alloys [22] and zirconium [57], $a+c$ dislocations are confined in $\{10\bar{1}\}$ slip bands, and segments parallel to $\langle 11\bar{2}0 \rangle$ directions are predominant. In magnesium, the configuration of dislocations associated with the $\{11\bar{2}\}$ slip has been shown to depend upon the temperature of deformation. While the dislocations are mostly in the screw orientation when deformed below room temperature, edge dislocations aligned in $\langle 10\bar{1}0 \rangle$ directions and dislocation loops are prevalent for deformation temperatures between room temperature and 380 K [54]. By electron microscopy it was found [54] that the edge dislocations in magnesium are dissociated as follows:

$$\frac{1}{3}\langle \bar{1}\bar{1}23 \rangle \rightarrow \frac{1}{6}\langle \bar{2}023 \rangle + \frac{1}{6}\langle 0\bar{2}23 \rangle. \quad (5)$$

partial dislocations to cross-glide onto the basal plane because they have no edge component in their Burgers vectors. If a leading partial dislocation happens to cross-glide onto the basal plane (e.g., with the aid of thermal energy) in the course of the prismatic glide, the velocity will be much reduced because it is always the case in experiments for prismatic slip that the shear stress acting on the basal plane is very small. In beryllium, the CRSS for the prismatic slip is known to exhibit an anomalous increase in the temperature range from 200 K to 450 K [38,41]. Regnier and Dupouy [41] proposed a model to account for the phenomenon: the screw dislocations on prismatic planes are dissociated into pure screw partial dislocations, and with increasing temperature these partial dislocations begin to cross-glide onto the basal plane by thermal activation to become eventually immobile. The result of the simulation for beryllium thus supports this model.

Since this dissociation occurs on the basal plane (i.e., out of the glide plane), the dislocation in this configuration cannot glide on $\{11\bar{2}\}$. It was proposed to be this sessile dissociation that is responsible for the increase in the CRSS in this temperature range (Fig. 8). Similar increase in the CRSS for $\{11\bar{2}\}$ slip has been observed for zinc [58] and cobalt [59].

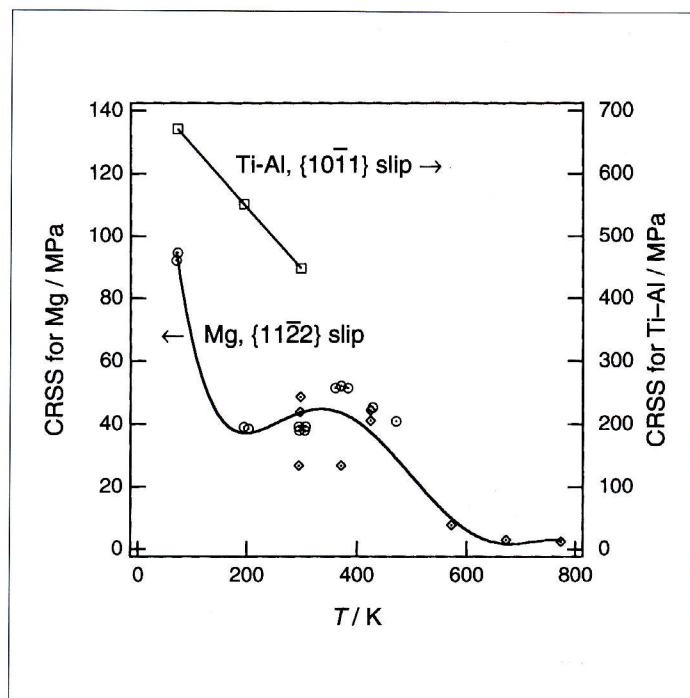
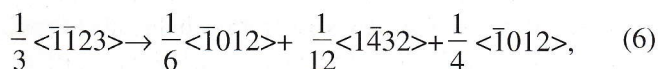


Figure 8: Critical resolved-shear-stress (CRSS) for the $\{11\bar{2}\}\langle \bar{1}\bar{1}23 \rangle$ slip in magnesium [54,55] and that for the $\{10\bar{1}\}\langle \bar{1}\bar{1}23 \rangle$ slip in a titanium–aluminium (7 mol %) solid solution alloy [56]

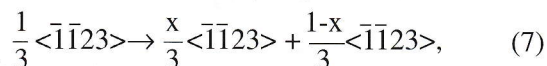
Stacking faults and dissociation models

The Burgers vector of $\mathbf{a+c}$ dislocations is almost twice as large as a dislocations, and the spacings of the glide planes, $\{10\bar{1}1\}$ and $\{11\bar{2}2\}$, are smaller than those of the primary slip planes (the basal or prismatic planes) by 10% and 50%, respectively. As a result, theoretically calculated Peierls stress amounts to 0.1μ for the $\{10\bar{1}1\}$ glide and 0.4μ for the $\{11\bar{2}2\}$ glide [60]. It was thus difficult to imagine that the dislocations glide in the form of a perfect dislocation; dissociation into partial dislocations seemed prerequisite.

Figures 9 and 10 show atomic arrangements in $\{10\bar{1}1\}$ and $\{11\bar{2}2\}$ planes. The hard-sphere model predicted [40] that two stacking faults would exist on $\{10\bar{1}1\}$, whereby $\mathbf{a+c}$ dislocations might dissociate into three partial dislocations, as indicated by the arrows in Fig. 9. The dissociation can be written as



where components perpendicular to the glide plane [8] have been omitted for the sake of simplicity. These two faults, referred to as F_1 and F_2 , have been found to be stable in atomistic simulation [42,43,52], with the energy of F_1 being lower than that of F_2 . Their positions and relative magnitudes of the energies do not depend much on potentials. In simulation studies [42,43,52,61], a stacking fault on $\{11\bar{2}2\}$ has also been found at a position dividing the $\mathbf{a+c}$ vector into 1:1 or 1:3, the exact location depending upon the potential used. The energy of the fault is similar in magnitude to the energy of F_2 on $\{10\bar{1}1\}$. Owing to the presence of the fault, the following dissociation on $\{11\bar{2}2\}$ is possible:



where x is in the range between $1/4$ and $1/2$.

Core structures and glide mechanisms

Minonishi and coworkers studied the core structures and glide mechanisms of the $\mathbf{a+c}$ screw dislocation and the edge dislocation on $\{11\bar{2}2\}$ using the Lennard-Jones potential [61–64]. The screw dislocation of the Burgers vector $1/3[\bar{1}\bar{1}23]$ was found to extend over either $(10\bar{1}1)$, $(01\bar{1}1)$ or $(11\bar{2}2)$ (for which $[\bar{1}\bar{1}23]$ is the common zone axis), or over two planes of the three. The structures of the cores extended over a single plane (of $\{10\bar{1}1\}$ type or $\{11\bar{2}2\}$ type) can be interpreted as the dissociation (6) or (7). The screw dislocation glides on planes of $\{10\bar{1}1\}$ type under the external shear stress that arises under c -axis tension, whereas it glides on planes of $\{11\bar{2}2\}$ type under the shear stress that arises under c -axis compression. This response to the stresses of opposite senses is independent of the initial core configuration and of the plane of the shear.

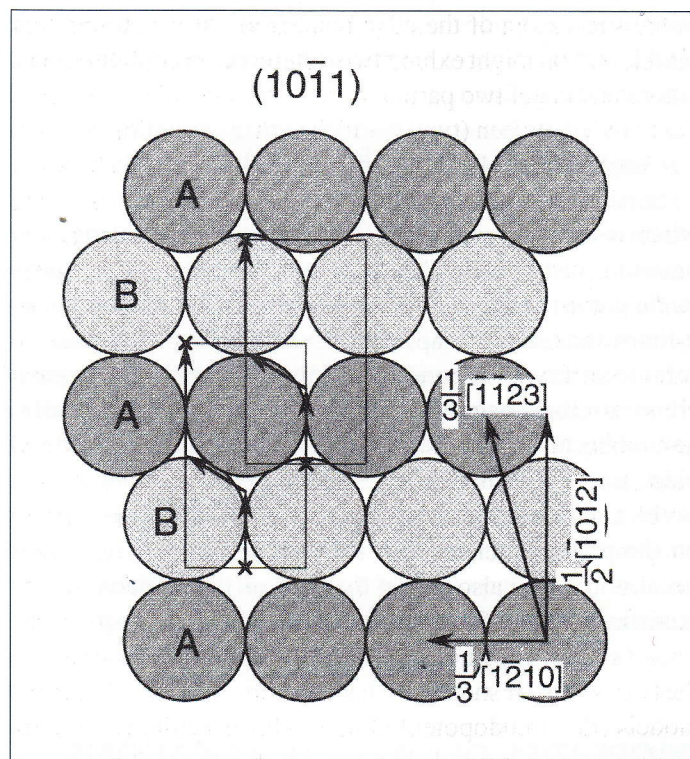


Figure 9: Atomic arrangement of the $(10\bar{1}1)$ pyramidal plane. Atom rows B are located below rows A by $1/6$ times the interplanar spacing. Crosses indicate the positions of atoms in the next plane. Arrows in the rectangle represent the dissociation of the $\mathbf{a+c}$ dislocation according to reaction (6)

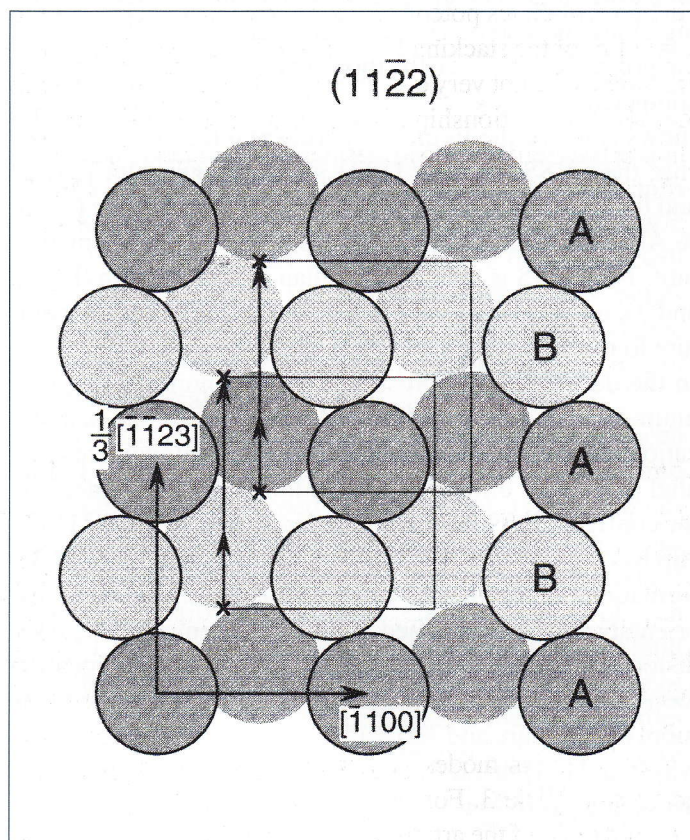


Figure 10: Atomic arrangement of the $(11\bar{2}2)$ pyramidal plane. Circles not delineated are atoms in the plane below. Arrows represent the dissociation of the $\mathbf{a+c}$ dislocation according to reaction (7)

In the simulation of the edge dislocation, it was found that the dislocation might exhibit two different core configurations, one consisting of two partial dislocations and a $\{11\bar{2}2\}$ stacking fault in between (type I) and the other consisting of small $\{11\bar{2}1\}$ and $\{11\bar{2}2\}$ twin structures (type II). The dislocation of type I configuration glides on $\{11\bar{2}2\}$, regardless of the sense of shear stress. That of type II configuration also glides on $\{11\bar{2}2\}$ under the shear stress corresponding to c axis compression, but a $\{11\bar{2}1\}$ twin develops when the shear of the opposite sense is applied. The behaviour of the dislocation with type II core is indicative of the experimental observation on magnesium and zinc: these metals deform by $a+c$ slip under compression along the c axis but $\{11\bar{2}1\}$ twinning is activated under tension along the c axis. Both the simulation and experiment suggest that $a+c$ slip and twinning are closely related to each other at an atomistic level. Liang and Bacon also studied $a+c$ dislocations using the pair-potential models [34,35]. Their results are substantially the same as those of Minonishi et al., except that the response to the two senses of shear stresses is reversed in one of the four models (the pseudopotential model for beryllium). The behaviour of $a+c$ screw dislocations in the Finnis-Sinclair potential models for magnesium and titanium has been examined by the present authors [65]. The core structure and the mechanism of glide motion of the screw dislocation have again been found to be essentially similar to those obtained with the Lennard-Jones potential. This is reasonable because the properties of the stacking faults in the Finnis-Sinclair potential models are not very different from those of pair potential models. The relationship between the sense of shear and the glide plane depends, however, upon potentials. The screw dislocation in the model of titanium glides either on $\{10\bar{1}1\}$ or on $\{11\bar{2}2\}$, depending upon the direction of the stress in

the same way as the case of the Lennard-Jones potential, whereas the dislocation in the model of magnesium glides on planes of $\{10\bar{1}1\}$ type, irrespective of the sense of the shear. The results of simulation on screw dislocations obtained with various interatomic interaction models indicate that the energy difference between dissociation schemes (6) and (7) is minor, and the glide plane of $a+c$ dislocations may change, depending sensitively upon subtle differences in interatomic forces and/or stress states. In experiment, both $\{10\bar{1}1\}$ glide and $\{11\bar{2}2\}$ glide have been observed for titanium. This suggests that the stability of the dislocation extended on $\{10\bar{1}1\}$ and that on $\{11\bar{2}2\}$ are actually close to each other in this material.

The present authors studied the core structure of the $a+c$ dislocation for various orientations on $\{1\bar{2}01\}$ [66,67], which is the glide plane of the dislocation in titanium and zirconium. The dislocation in the $[\bar{1}210]$ direction exhibits a non-planar core, which involves an edge partial dislocation, a wide ribbon of the fault F_1 and a non-planar partial dislocation, as the stable form. For other orientations, the dislocation is dissociated into two partial dislocations with the low-energy fault F_1 , or into three partial dislocations with F_1 and F_2 as in (6), and the total dislocation glides under external stress by retaining the stress-free core configuration. The dislocation in the $[\bar{1}210]$ direction has been found to be far less mobile; it begins to glide only after transforming to the planar core composed of the three partial dislocations. The arrangement of dislocations observed in titanium, titanium-aluminium alloys and zirconium can be explained by the low mobility of the dislocation in this orientation: the predominance of the segments aligned in this orientation could result from the non-planar core configuration.

DISLOCATIONS IN DO_{19} ORDERED ALLOYS AND INTERMETALLIC COMPOUNDS

Crystal structure and deformation modes [68]

The DO_{19} structure is an ordered structure based on the hcp lattice with the stoichiometry of A_3B . Figure 11 shows the atomic arrangement in the unit cell. The periodicity in the basal plane is twice as long as that in the hcp lattice, while the c axis remains the same. The alloys and compounds of this structure involve Mg_3Cd , Cd_3Mg , Ti_3Al , Ti_3Sn and Mn_3Sn .

The deformation modes of some DO_{19} type alloys are summarized in Table 3. For the sake of compatibility with the foregoing part of the article, Miller-Bravais indices based on the fundamental hcp lattice are adopted. The primary mode of plastic deformation is the slip due to dislocations with the Burgers vector $2a$ along the basal plane or along the $\{10\bar{1}0\}$

prismatic plane. In Mg_3Cd and Cd_3Mg , which are order-disorder type alloys, basal slip is the easiest in the disordered state, whereas basal slip and prismatic slip become equally active upon ordering. In Mg_3Cd , slip in the $a+c$ direction on $\{10\bar{1}1\}$ and $\{11\bar{2}2\}$ planes also take place. Ti_3Al and Ti_3Sn deform primarily by prismatic slip in the same way as titanium. The $\{11\bar{2}2\}$ pyramidal slip is known to occur under c -axis compression in these materials. However, 2 ($a+c$) dislocations have recently been found to glide on $\{10\bar{1}1\}$ under c -axis tension [69].

It is noteworthy that anomalous increase in the flow stress with temperature is observed for a number of slip systems, e.g., the basal slip in Mg_3Cd , Cd_3Mg and Mn_3Sn , and the

TABLE 3 - Slip modes of the ordered alloys and intermetallic compounds of the DO_{19} structure. Crystallographic planes and directions are represented by Miller-Bravais indices for the fundamental hcp lattice

Material	Primary mode(s)	Secondary mode(s)
Mg_3Cd	$(0002)\langle 1\bar{2}10\rangle, \{10\bar{1}0\}\langle 1\bar{2}10\rangle$	$\{10\bar{1}1\}^\dagger, \{11\bar{2}2\}^\dagger$
Cd_3Mg	$(0002)\langle 1\bar{2}10\rangle, \{10\bar{1}0\}\langle 1\bar{2}10\rangle$	
Ti_3Al	$\{10\bar{1}0\}\langle 1\bar{2}10\rangle$	$(0002)\langle 1\bar{2}10\rangle, \{11\bar{2}2\}\langle 11\bar{2}3\rangle, \{10\bar{1}1\}\langle 11\bar{2}3\rangle$
Ti_3Sn	$\{10\bar{1}0\}\langle 1\bar{2}10\rangle$	$\{10\bar{1}1\}\langle 1\bar{2}10\rangle, (0002)\langle 12\bar{1}0\rangle$
Mn_3Sn	$(0002)\langle 1\bar{2}10\rangle$	$\{10\bar{1}0\}\langle 1\bar{2}10\rangle, \{10\bar{1}1\}\langle 11\bar{2}3\rangle$

[†] Neither the macroscopic slip direction nor the Burgers vector of the dislocations has been identified.

$\{11\bar{2}2\}$ pyramidal slip in Ti_3Al . For the cases of Mg_3Cd and Cd_3Mg , the anomaly is attributed to the order-disorder transformation. On the other hand, the phenomenon in Ti_3Al is believed to be associated with complex dissociation of $2(\mathbf{a}+\mathbf{c})$ dislocations, as will be described later. Another point to be noted is that deformation twinning scarcely occurs in DO_{19}

alloys and compounds. In Mg_3Cd , for example, $\{10\bar{1}2\}$ twinning is the principal deformation mode contributing to the strain in the c axis in the disordered state, but it is replaced by $\{11\bar{2}2\}$ slip due to $2(\mathbf{a}+\mathbf{c})$ dislocations in the ordered state. The role of the pyramidal slip in the ductility of these materials is therefore very important.

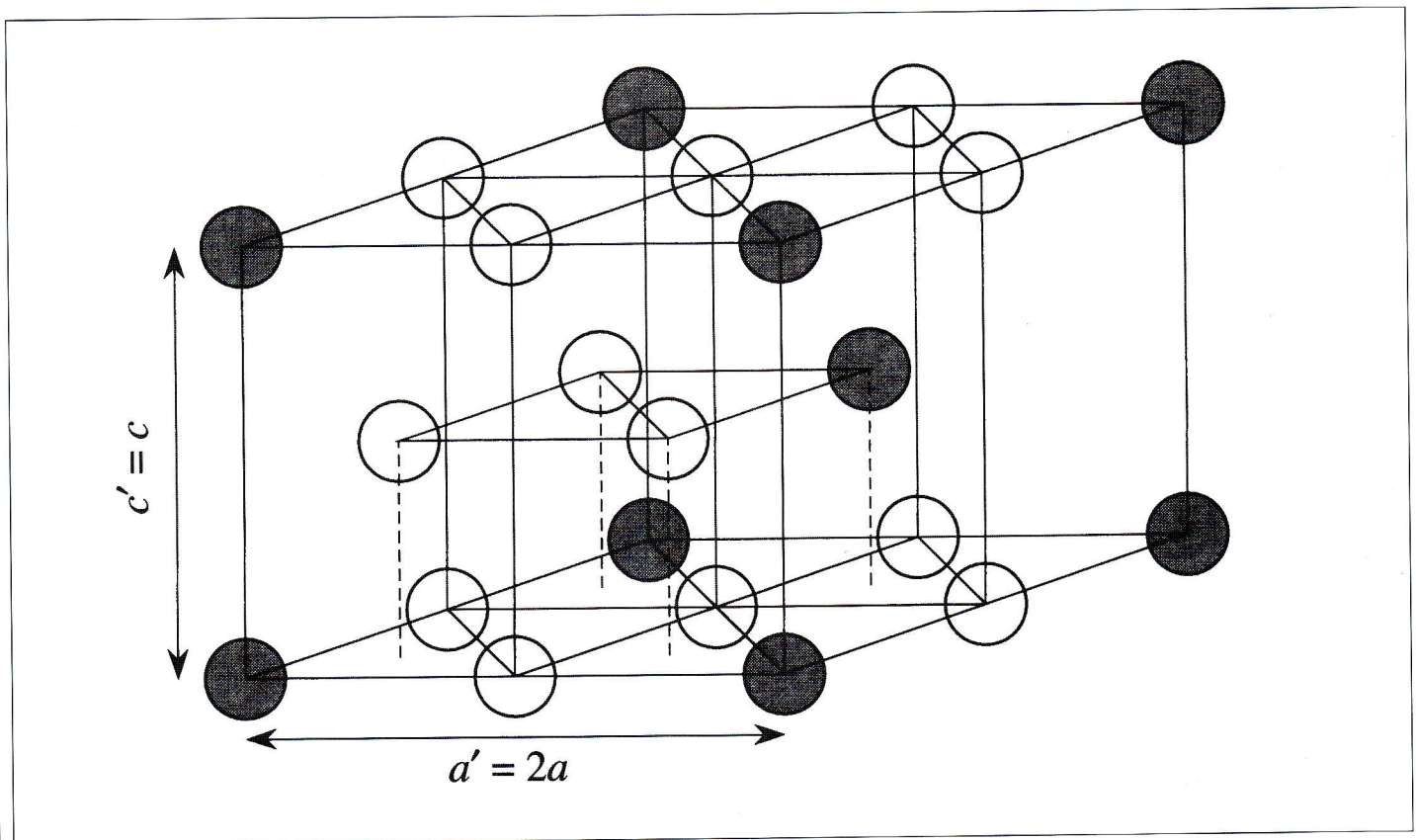


Figure 11: Unit cell of the DO_{19} ordered structure for A_3B alloys. Open circles: A atoms, filled circles: B atoms. a, c : lattice parameters for the fundamental hcp cell, a', c' : lattice parameters for the DO_{19} cell

Planar faults

In crystals of ordered structures, various types of planar faults exist: anti-phase boundaries (APB), superlattice intrinsic stacking faults (SISF) and complex stacking faults (CSF). A classified list of planar faults in the DO_{19} structure is given by Umakoshi and Yamaguchi [70]. Figure 12 is a projection of the atomic arrangement in the perfect crystal onto the basal plane. The three vectors in the figure, $\mathbf{b}_A = 1/3[11\bar{2}0]$, $\mathbf{b}_S = 2/3[10\bar{1}0]$ and $\mathbf{b}_C = 1/3[01\bar{1}0]$, are the translation vectors for the APB, SISF and CSF, respectively, on the basal plane. The SISF on the basal plane is the counterpart of the stacking fault I_2 in the hcp structure and is always stable owing to the symmetry of the crystal. On the other hand, the stability of the APB and that of the CSF depend upon interatomic interactions, and their positions may deviate from the above, laterally for \mathbf{b}_A or longitudinally for \mathbf{b}_C . The APB on the prismatic plane is created by the same translation vector \mathbf{b}_A ($= 1/3[11\bar{2}0]$), and is guaranteed to be a stable fault by symmetry. Two types of $\{10\bar{1}0\}$ APBs may exist, I and II, depending upon the positions of the cut, as indicated by arrows in the figure. Since the atomic arrangements at the nearest neighbour positions are not disturbed in the APB of type I, its energy is expected to be lower than that of type II APB. Cserti, Khanta, Vitek and Pope [71] modelled planar faults

and dislocations in a DO_{19} alloy using Finnis-Sinclair type potentials. They first examined the stability of APBs and stacking faults on the basal plane and on the prismatic plane. The APB, SISF and CSF on the basal plane have been found to be stable, with the energy being the lowest for the SISF. The positions of the APB and CSF have been shown to be close to those in Fig. 12. The energies of the faults are listed in Table 4. According to these results, $2a$ dislocations on the basal plane may dissociate into either (a) superlattice Shockley partial dislocations bounding the SISF, (b) two superpartial dislocations bounding the APB, or (c) four partial dislocations bounding the CSF, APB and CSF. Concerning the faults on the prismatic plane, the energy of the APB of type I is lower than that of type II, as expected, by nearly an order of magnitude. In addition, a CSF has been found to exist on the prismatic plane. It is located at a position close to the $1/6\langle 11\bar{2}1 \rangle$ fault in hcp crystals and its energy is slightly higher than the APB of type II. It is therefore possible for a $2a$ dislocation to dissociate on the prismatic plane into (a) two superpartial dislocations bounding an APB (of type I or of type II) or (2) four partial dislocations bounding the CSF, APB and CSF.

To the authors' knowledge, no atomistic studies on planar faults on planes other than the basal and prismatic planes have been reported.

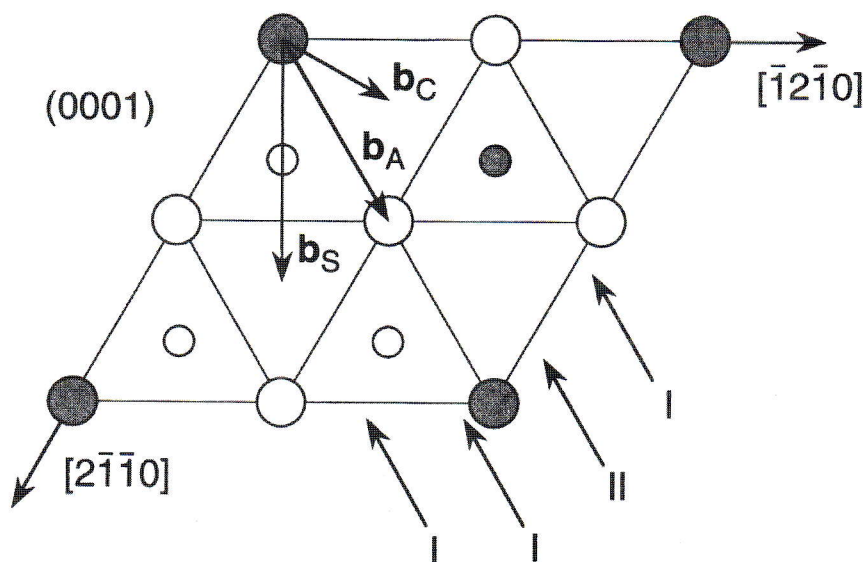


Figure 12: Projection of the atomic arrangement in the DO_{19} structure onto the basal plane. Large circles and small circles differ in their positions in the direction normal to the paper by $c/2$. \mathbf{b}_A , \mathbf{b}_S and \mathbf{b}_C are displacement vectors for creating the APB, SISF and CSF, respectively, on the basal plane. Two types of APBs are produced by shifting the neighbouring prismatic planes by \mathbf{b}_A ; the positions of the cut-plane for type I and type II APB are indicated

TABLE 4 - Calculated energies of the planar faults in a model DO_{19} crystal [71] and experimental values for Ti_3Al [79]. Units: $10^{-3}Gmk$ (μ : the shear modulus, a : the interatomic distance in the basal plane)

Crystal	Basal plane			Prismatic plane		
	APB	SISF	CSF	APB-I	APB-II	CSF
Model	4.59	3.26	6.12	0.816	7.36	9.64
Ti_3Al	3.7	4.0	-	2.4	4.9	-

Dislocations in Ti_3Al

In recent years, microscopic aspects of dislocations in Ti_3Al have been studied in detail by transmission electron microscopy [69,72–81]. The dislocations responsible for the prismatic slip, with the total Burgers vector $2a$, have been shown to be predominantly in the screw orientation in materials deformed below room temperature [76]. However, with increasing temperature the prevalence of the screw orientation disappears and edge dislocations become dominant instead [74,76]. The $2a$ dislocations are dissociated at all temperatures into two superpartial dislocations separated by an APB on the prismatic plane [74,76]. Legros, Couret and Caillard [79] observed two distinctly different separations between the superpartial dislocations, even along a single dislocation. They interpreted the narrowly and widely separated parts as the APB of type II and that of type I, respectively, and estimated the APB energies to be 84 and 42 mJ/m². They also evaluated the energies of the APB and SISF on the basal plane from observations of screw dislocations extended on the basal plane. The energies of the faults thus estimated are compared with the values calculated by Cserti et al. in Table 4. The experimental and calculated energies of each fault are of the same order of magnitude.

Electron microscopy studies have been performed also on $2(a+c)$ dislocations in Ti_3Al , which are responsible for the pyramidal slip. As mentioned earlier, the CRSS for the $\{11\bar{2}\}$ slip under compression along the c axis increases from room temperature and exhibits a peak at 700°C [73]. The dislocations are mostly of screw character at low temperatures [76]

but edge dislocations prevail at room temperature and above [73]. The superdislocations are dissociated at all temperatures into superpartial dislocations with a Burgers vector $a+c$ [76,78]. The observed widths of the APB on $\{11\bar{2}\}$ separating the superpartial dislocations scatter considerably, however, thus allowing no reliable estimate of the APB energy. A recent electron microscopy study [75] has demonstrated that the Burgers vectors of the superpartial dislocations are of the same sense when deformation is done at temperatures below 500°C, whereas they are of opposite senses at temperatures around 700°C. Furthermore, the superdislocations are dissociated on the basal plane according to reaction (5), similarly to the $a+c$ edge dislocations in magnesium [54]. These experimental observations indicate that the strength anomaly is related to the sessile dissociation of the superpartial dislocations. However, the exact origin of the variation of the dislocation configurations with temperature is yet unclear; further studies are necessary for clarifying the mechanism of the strengthening.

For $2(a+c)$ dislocations in Ti_3Al , there are still some other interesting features reported: (a) unlike the basal slip and the prismatic slip, the CRSS of the $\{11\bar{2}\}$ slip depends strongly upon the composition [82], and (b) the dislocations glide not on $\{11\bar{2}\}$ but on $\{10\bar{1}\}$ under tension along the c axis [69]. To understand such phenomena, particularly the latter, atomistic studies of planar faults and dislocations must be useful.

SUMMARY AND CONCLUDING REMARKS

Theoretical calculations of stacking fault energies and atomistic simulation of dislocations have provided important information for better understanding the wide spectrum of the deformation behaviour of hcp metals. Since stacking faults have decisive effects on the properties of dislocations, investigations of the stability of planar faults are expected to give an essential clue, and it is actually the case for the study of dislocations hcp metals. The relative ease the basal slip and the prismatic slip in various metals has been explained from the stability of the stacking faults relevant to a dislocations. Simulation studies suggest that the dislocations in basal-slip metals are dissociated on the basal plane into Shockley partial dislocations, whereas in prismatic-slip metals they are predicted to have non-planar core structures. The magnitudes of the CRSS and their variations with temperature can also

be understood from the core structures. Computer simulations have also helped envisage possible atomic structures of $\mathbf{a+c}$ dislocations and their glide mechanisms on pyramidal planes. Studies on the atomic structure of planar faults and dislocations will also be useful for D0_{19} alloys and compounds. From an experimental standpoint, there still remain important issues in the plasticity of hcp metals. Some of such issues are (a) the effects of interstitial solute elements such as oxygen and nitrogen, which are very difficult to reduce, in refractory hcp metals, titanium, zirconium and hafnium, and (2) the failure of Schmid's law for the prismatic slip in titanium [23]. To solve these problems, careful experiments on materials of controlled purity are desirable.

ACKNOWLEDGMENTS

The authors are indebted to Dr Y. Minonishi (Tohoku University) for discussion and comments, to Messrs A. Yamanaka and T. Ando for their cooperation in the experimental and simulation studies. They also wish to thank Kawakami Memorial Foundation for financial support.

REFERENCES

- [1] Minonishi, Y., Core structures of dislocations in hcp metals. *Bull. Japan Inst. Metals*, 23 (1984), 515-522 (in Japanese).
- [2] Vitek, V., Effect of dislocation core structure on the plastic properties of metallic materials. In *Dislocations and Properties of Real Materials*, The Institute of Metals, London, 1985, pp. 30-50.
- [3] Partridge, P. G., The crystallography and deformation modes of hexagonal close-packed metals. *Metall. Rev.*, 118 (1967), 169-194.
- [4] Conrad, H., Effect of interstitial solutes on the strength and ductility of titanium. *Prog. Mater. Sci.*, 26 (1981), 123-403.
- [5] Mahajan, S. and D. F. Williams, Deformation twinning in metals and alloys. *Int. Metall. Rev.*, 18 (1973), 43-61.
- [6] Yoo, M. H., Slip, twinning and fracture in hexagonal close-packed metals. *Metall. Trans. A*, 12A (1981), 409-418.
- [7] Morris, J. R., Y. Y. Ye, K. M. Ho, C. T. Chan and M. H. Yoo, Structures and energies of compression twin boundaries in hcp Ti and Zr. *Phil. Mag. A*, 72 (1995), 751-763.
- [8] Jones, I. P. and W. B. Hutchinson, Stress-state dependence of slip in titanium-6Al-4V and other h.c.p. metals. *Acta Metall.*, 29 (1981), 951-968.
- [9] Numakura, H., Y. Minonishi and M. Koiwa, $\langle \bar{1}\bar{1}23 \rangle \{10\bar{1}1\}$ slip in titanium polycrystals at room temperature. *Scripta Metall.*, 20 (1986), 1581-1586.
- [10] Minonishi, Y., S. Morozumi and H. Yoshinaga, $\{\bar{1}\bar{1}22\} \langle 11\bar{2}3 \rangle$ slip in titanium. *Scripta Metall.*, 16 (1982), 427.
- [11] Tan, X., H. Gu, S. Zhang and C. Laird, Loading mode dependence of deformation microstructure in a high-purity titanium single crystal oriented for difficult glide. *Mater. Sci. Engng*, A189 (1994), 77-84.
- [12] Sheely, W. F. and R. R. Nash, Mechanical properties of magnesium monocrystals. *Trans. Metall. Soc. AIME*, 218 (1960), 416-423.
- [13] Flynn, P. W., J. Mote and J. E. Dorn, On the thermally activated mechanism of prismatic slip in magnesium single crystals. *Trans. Metall. Soc. AIME*, 221 (1961), 1148-1154.
- [14] Akhtar, A. and E. Teghtsoonian, Solid solution strengthening of magnesium single crystals - II The effect of solute on the ease of prismatic slip. *Acta Metall.*, 17 (1969), 1351-1356.
- [15] Levine, E. D., Deformation mechanisms in titanium at low temperatures. *Trans. Metall. Soc. AIME*, 236 (1966), 1558-1565.
- [16] Tanaka, T. and H. Conrad, Deformation kinetics for $\{10\bar{1}0\} \langle 11\bar{2}0 \rangle$ slip in titanium single crystals below $0.4T_m$. *Acta Metall.*, 20 (1972), 1019-1029.
- [17] Akhtar, A. and E. Teghtsoonian, Prismatic slip in α -titanium single crystals. *Metall. Trans.*, 6A (1975), 2201-2208.
- [18] Akhtar, A., Basal slip and twinning in α -titanium single crystals. *Metall. Trans.*, 6A (1975), 1105-1113.
- [19] Biget, M. P. and G. Saada, Low-temperature plasticity of high-purity α -titanium single crystals. *Phil. Mag. A*, 59 (1989), 747-757.
- [20] Hirsch, P. B. and J. S. Lally, The deformation of magnesium single crystals. *Phil. Mag.*, 12 (1965), 595-648.
- [21] Sharp, J. V., M. J. Makin and J. W. Christian, Dislocation structure in deformed single crystals of magnesium. *Phys. Stat. Sol.*, 11 (1965), 845-864.
- [22] Cass, T. R., Slip modes and dislocation substructures in titanium and titanium-aluminum single crystals. In R. I. Jaffee and N. E. Promisel (Eds.), *The Science, Technology and Application of Titanium*, Pergamon, Oxford, 1970, pp. 459-477.
- [23] Naka, S., A. Lasalmonie, P. Costa and L. P. Kubin, The low-temperature plastic deformation of α -titanium and the core structure of \mathbf{a} -type screw dislocations. *Phil. Mag. A*, 57 (1988), 717-740.

- [24] Tyson, W., Basal and prismatic slip in h.c.p. crystals. *Acta Metall.*, 15 (1967), 574-577.
- [25] Yoo, M. H. and C. T. Wei, Slip modes of hexagonal-close-packed metals. *J. Appl. Phys.*, 38 (1967), 4317-4322.
- [26] Hirth, J. P. and J. Lothe, *Theory of Dislocations*, Second Ed., John Wiley & Sons, New York, 1982, pp. 354-366.
- [27] Korner, A. and H. P. Karnthaler, Weak-beam study of glide dislocations in h.c.p. cobalt. *Phil. Mag. A*, 48 (1983), 469-477.
- [28] Fleischer, R. L., Stacking fault energies of hcp metals. *Scripta Metall.*, 20 (1986), 223-224.
- [29] Chetty, N. and M. Weinert, Stacking faults in magnesium. *Phys. Rev. B*, 56 (1997), 10844-10851.
- [30] Basinski, Z. S., M. S. Duesbery and R. Taylor, Screw dislocation in a model sodium lattice. *Phil. Mag.*, 21 (1971), 1201-1221.
- [31] Basinski, Z. S., M. S. Duesbery and R. Taylor, Influence of shear stress on screw dislocations in a model sodium lattice. *Can. J. Phys.*, 49 (1971), 2160-2180.
- [32] Bacon, D. J. and J. W. Martin, The atomic structure of dislocations in h.c.p. metals I. Potentials and unstressed crystals. *Phil. Mag. A*, 43 (1981), 883-900.
- [33] Bacon, D. J. and J. W. Martin, The atomic structure of dislocations in h.c.p. metals II. Behaviour of the core under an applied stress. *Phil. Mag. A*, 43 (1981), 901-909.
- [34] Liang, M. H., and D. J. Bacon, Computer simulation of dislocation cores in h.c.p. metals II. Core structure in unstressed crystals. *Phil. Mag. A*, 53 (1986), 181-204.
- [35] Liang, M. H., and D. J. Bacon, Computer simulation of dislocation cores in h.c.p. metals III. The effect of applied shear strain. *Phil. Mag. A*, 53 (1986), 205-220.
- [36] Escaig, B., L'activation thermique des déviations sous faibles contraintes dans les structures h.c. et c.c. *Phys. Stat. Sol.*, 28 (1968), 463-474.
- [37] Yoshinaga, H. and R. Horiuchi, On the nonbasal slip in magnesium crystals. *Trans. Japan Inst. Metals*, 5 (1964), 14-21.
- [38] Couret, A., D. Caillard, W. Püschl and G. Schoeck, Prismatic glide in divalent h.c.p. metals. *Phil. Mag. A*, 63 (1991), 1045-1057.
- [39] Churchman, A. T., The slip modes of titanium and the effect of purity on their occurrence during tensile deformation of single crystals. *Proc. Roy. Soc. A*, 226 (1954), 216-226.
- [40] Rosenbaum, H. S., Nonbasal slip in h.c.p. metals and its relation to mechanical twinning. In R. E. Reed-Hill, J. P. Hirth and H. C. Rogers (Eds.), *Deformation Twinning*, Gordon & Breach, New York, 1964, pp. 43-76.
- [41] Regnier, P. and J. M. Dupouy, Prismatic slip in beryllium and the relative ease of glide in h.c.p. metals. *Phys. Stat. Sol.*, 39 (1970), 79-93.
- [42] Schwartzkopff, K., Metastable stacking sequences in hexagonal metals. *Acta Metall.*, 17 (1969), 345-351.
- [43] Bacon, D. J. and M. H. Liang, Computer simulation of dislocation cores in h.c.p. metals I. Interatomic potentials and stacking-fault stability. *Phil. Mag. A*, 53 (1986), 163-179.
- [44] Numakura, H., unpublished work.
- [45] In atomistic simulations by the method of molecular statics, the energy map for translational faults is often calculated by allowing atoms to relax only in the direction perpendicular to the plane of the fault. To accurately determine the position and energy of a stacking fault, however, atoms should be relaxed freely. This is particularly important for planes other than the basal plane in hcp crystals, where in-plane displacements and accommodations between non-equivalent atoms ('shuffling') are expected to occur and may have a significant effect. Concerning the stacking faults discussed in the present article, the difference between the cases with one and three degrees of freedom in the relaxation is small except for the fault on {1122} with the Lennard-Jones potential [44]. This problem has also been discussed by: Morris, J. R., J. Scharff, K. M. Ho, D. E. Turner, Y. Y. Ye and M. H. Yoo, Prediction of a {1122} hcp stacking fault using a modified generalized stacking-fault calculation. *Phil. Mag. A*, 76 (1997), 1065-1077.
- [46] de Crecy, A., A. Bourret, S. Naka and A. Lasalmonie, High resolution determination of the core structure of $1/3\langle 11\bar{2}0 \rangle\{10\bar{1}0\}$ edge dislocation in titanium. *Phil. Mag. A*, 47 (1983), 245-254.
- [47] Akhtar, A. and E. Teghtsoonian, Plastic deformation of zirconium single crystals. *Acta Metall.*, 19 (1971), 655-663.
- [48] Legrand, B., Structure du coeur des dislocations vis $1/3\langle 11\bar{2}0 \rangle$ dans le titane. *Phil. Mag. A*, 52 (1985), 83-97.
- [49] Farenc, S., D. Caillard and A. Couret, An *in-situ* study of prismatic glide in titanium at low temperatures. *Acta Metall. Mater.*, 41 (1993), 2701-2709.
- [50] Legrand, B., Relations entre la structure électronique et la facilité de glissement dans les métaux hexagonaux compacts. *Phil. Mag. B*, 49 (1984), 171-184.
- [51] Igarashi, M., M. Khantha and V. Vitek, *N*-body interatomic potentials for hexagonal close-packed metals. *Phil. Mag. B*, 63 (1991), 603-627.
- [52] Igarashi, M., Doctor Thesis, Atomistic studies on extended lattice defects in h.c.p. metals. Graduate School of Engineering, Kyoto University, Kyoto, 1991.
- [53] Vitek, V. and M. Igarashi, Core structure of $1/3\langle 11\bar{2}0 \rangle$ screw dislocations on basal and prismatic planes in h.c.p. metals: an atomistic study. *Phil. Mag. A*, 63 (1991), 1059-1075.
- [54] Stohr, J. F. and J. P. Poirier, Etude en microscopie électronique du glissement pyramidal $\{11\bar{2}2\}\langle 11\bar{2}3 \rangle$ dans le magnésium. *Phil. Mag.*, 25 (1972), 1313-1329.
- [55] Obara, T., H. Yoshinaga and S. Morozumi, $\{11\bar{2}2\}\langle 11\bar{2}3 \rangle$ slip system in magnesium. *Acta Metall.*, 21 (1973), 845-853.
- [56] Paton, N. E., J. C. Williams and G. P. Rauscher, The deformation of α -phase titanium. In R. I. Jaffee and H. M. Burte (Eds.), *Titanium Science and Technology*, Plenum, New York, 1973, pp. 1049-1069.
- [57] H. Numakura, Y. Minonishi and M. Koiwa, $\langle 11\bar{2}3 \rangle\{10\bar{1}1\}$ slip in zirconium. *Phil. Mag. A*, 63 (1991), 1077-1084.
- [58] Blish, R. C., II and T. Vreeland, Jr., Dislocation velocity on the $\{112\}\langle 1213 \rangle$ slip systems of zinc. *J. Appl. Phys.*, 40 (1969), 884-890.
- [59] Akhtar, A., Pyramidal slip in cobalt. *Scripta Metall.*, 10 (1976), 365-366.
- [60] Numakura, H., M. Koiwa, T. Ando and M. H. Yoo, Effects of elastic anisotropy on the properties of *a+c* dislocations in h.c.p. metals. *Mater. Trans. JIM*, 33 (1992), 1130-1137.
- [61] Minonishi, Y., S. Ishioka, M. Koiwa, S. Morozumi and M. Yamaguchi, The core structure of a $1/3\langle 11\bar{2}3 \rangle$ screw dislocation in h.c.p. metals. *Phil. Mag. A*, 44 (1981), 1225-1237.
- [62] Minonishi, Y., S. Ishioka, M. Koiwa, S. Morozumi and M. Yamaguchi, The core structure of $1/3\langle 11\bar{2}3 \rangle\{1122\}$ edge dislocations in h.c.p. metals. *Phil. Mag. A*, 43 (1981), 1017-1026.
- [63] Minonishi, Y., S. Ishioka, M. Koiwa and S. Morozumi, Motion of a $1/3\langle 11\bar{2}3 \rangle$ screw dislocation in a model h.c.p. lattice. *Phil. Mag. A*, 46 (1982), 761-770.
- [64] Minonishi, Y., S. Ishioka, M. Koiwa, S. Morozumi, M. Yamaguchi, The core structures of a $1/3\langle 11\bar{2}3 \rangle\{1122\}$ edge dislocation under applied shear stresses in an h.c.p. model crystal. *Phil. Mag. A*, 45 (1982), 835-850.
- [65] Numakura, H. and M. Koiwa, *Collected Abstracts of 1993 Autumn Meeting of the Japan Institute of Metals*, 1993, pp. 374 (in Japanese).
- [66] Numakura, H., Y. Minonishi and M. Koiwa, Atomistic study of $1/3\langle 11\bar{2}3 \rangle\{10\bar{1}1\}$ dislocations in h.c.p. crystals I. Structure of the dislocation cores. *Phil. Mag. A*, 62 (1990), 525-543.
- [67] Numakura, H., Y. Minonishi and M. Koiwa, Atomistic study of $1/3\langle 11\bar{2}3 \rangle\{10\bar{1}1\}$ dislocations in h.c.p. crystals II. Motion of the dislocations. *Phil. Mag. A*, 62 (1990), 545-556.
- [68] Yamaguchi, M. and Y. Umakoshi, The deformation behaviour of intermetallic superlattice compounds. *Prog. Mater. Sci.*, 34 (1990), 1-148.
- [69] Legros, M., Y. Minonishi and D. Caillard, An *in-situ* transmission electron microscopy study of pyramidal slip in Ti_3Al . Geometry and kinetics of glide. *Phil. Mag. A*, 76 (1997), 995-1011.
- [70] Umakoshi, Y. and M. Yamaguchi, The stability and energies of planar faults in the DO_{19} ordered structure. *Phys. Stat. Sol. (a)*, 68 (1981), 457-468.
- [71] Cserti, J., M. Khanta, V. Vitek and D. P. Pope, An atomistic study of the dislocation core structures and mechanical behavior of a model DO_{19} alloy. *Mater. Sci. Eng.*, A152 (1992), 95-102.

- [72] Court, S. A., J. P. A. Löfvander, M. H. Loretto and H. L. Fraser, The influence of temperature and alloying additions on the mechanisms of plastic deformation of Ti_3Al . *Phil. Mag. A*, 61 (1990), 109-139.
- [73] Minonishi, Y. and M. H. Yoo, Anomalous temperature dependence of the yield stress of Ti_3Al by $\{11\bar{2}1\}\langle\bar{1}126\rangle$ slip. *Phil. Mag. Lett.*, 61 (1990), 203-208.
- [73] Minonishi, Y., Fourfold dissociation of $1/3\langle 1\bar{1}20\rangle$ superlattice dislocations in Ti_3Al . *Phil. Mag. Lett.*, 62 (1990), 153-158.
- [74] Minonishi, Y., Plastic deformation of single crystals of Ti_3Al with the $D0_{19}$ structure. *Phil. Mag. A*, 63 (1991), 1085-1093.
- [75] Minonishi, Y., In M. Yamaguchi and H. Fukutomi (Eds.), *Proc. 3rd Japan Int. SAMPE Symp. on Intermetallic Compounds for High-Temperature Structural Applications*, The Japan Chapter of SAMPE, Tokyo, 1993, pp. 1501-1506.
- [76] Inui, H., Y. Toda, Y. Shirai and M. Yamaguchi, Low-temperature deformation of single crystals of a $D0_{19}$ compound with an off-stoichiometric composition (Ti-36.5 at.% Al). *Phil. Mag. A*, 69 (1994), 1161-1177.
- [77] Minonishi, Y., In H. Oikawa et al. (Eds.), *Strength of Materials*, The Japan Institute of Metals, Sendai, 1994, pp. 129-132.
- [78] Minonishi, Y., Dissociation of $1/3\langle\bar{1}126\rangle\{1121\}$ superdislocations in Ti_3Al single crystals deformed at high temperatures. *Mater. Sci. Eng., A192/193* (1995), 830-836.
- [79] Legros, M., A. Couret and D. Caillard, Prismatic and basal slip in Ti_3Al I. Frictional forces on dislocations. *Phil. Mag. A*, 73 (1996), 61-80.
- [80] Legros, M., A. Couret and D. Caillard, Prismatic and basal slip in Ti_3Al II. Dislocation interactions and cross-slip processes. *Phil. Mag. A*, 73 (1996), 81-99.
- [81] Legros, M., Y. Minonishi and D. Caillard, An *in-situ* transmission electron microscopy study of pyramidal slip in Ti_3Al II. Fine structure of dislocations and dislocation loops. *Phil. Mag. A*, 76 (1997), 1013-1032.
- [82] Inui, H., Y. Toda, K. Kishida, Y. Shirai and M. Yamaguchi, Variation of CRSS for various slip systems with Al concentration in Ti_3Al single crystals. *J. Japan Inst. Metals*, 59 (1995), 586-587 (in Japanese).